Water Extraction of Airborne Polarimetric SAR by Introducing Eigenvalue Relative Difference

Zheng Changli, Zhang Wei, Ding Qing, Wang Xiaoxia, and Luo Jinghui

Abstract In high-resolution airborne SAR images, water bodies, paddy fields, roads, bare soils and other ground objects exhibit similar weak scattering characteristics. At present, the water body extraction algorithm based on the weak echo characteristics cannot eliminate the interference of other ground objects, resulting in unsatisfactory water extraction results. Aiming at the KU-band airborne polarimetric SAR image, this paper proposes a fine extraction method of airborne polarimetric SAR water with the relative difference of single-reflection eigenvalues. Firstly, the H-α Wishart classification algorithm is used to classify the weak scattering features, and then, the weakly scattered features are re-segmented based on the pre-classification results to construct the object unit. Finally, based on the single-reflex eigenvalue relative difference feature, the threshold method is used to realize the water fine extraction. Experiments show that the relative difference of single-reflection eigenvalues can effectively separate the water body from the rest of the weakly scattered features, and the object unit constructed by the fractal network evolution algorithm can obtain better water body fineness than the simple pixel-level analysis.

Keywords Polarimetric SAR · Water extraction · Object-oriented analysis · Speckle noise · Scattering characteristics

1 Introduction

Synthetic aperture radar (SAR) has the ability of all-day and all-weather surface observation. It can quickly respond to the severe weather conditions of rain, snow and fog and obtain the surface information of the target area. Water information plays an important role in flood assessment, urban management and river management. In recent years, with the development of airborne SAR system, UAV SAR with full polarization earth observation capability has played an important role in disaster prevention and mitigation. Compared with single-pol SAR system, full-pol SAR reveals the scattering difference of ground objects and provides a new technical

Z. Changli (✉) · Z. Wei · D. Qing · W. Xiaoxia · L. Jinghui
Science and Technology on Electronic Information Control Laboratory, 610036 Chengdu, China
e-mail: zs_zcl@163.com

L. Wang et al. (eds.), *Proceedings of the 6th China High Resolution Earth Observation Conference (CHREOC 2019)*, Lecture Notes in Electrical Engineering 657,
https://doi.org/10.1007/978-981-15-3947-3_43

means for the interpretation, classification and information extraction of ground objects.

At present, scholars at home and abroad mainly focus on four aspects [1–9]. (1) In view of the weak backscattering intensity of calm water surface and the characteristics of dark pixels in the image, water extraction research was carried out; (2) Research on water extraction based on the smooth texture characteristics of water body; (3) Study on water extraction based on the polarization characteristics of Bragg scattering; (4) Study on water extraction by mixing the bove characteristics. The above algorithms have achieved remarkable results in water extraction of spaceborne SAR images, but the results are not ideal for airborne SAR images. Compared with spaceborne SAR, airborne SAR has a larger incidence angle, which makes the water, paddy field, road and bare soil indistinguishable from airborne SAR images, and all of them have similar weak backscattering intensity characteristics. In addition, they all have smooth texture characteristics and odd scattering polarization characteristics, which make use of the above spaceborne SAR algorithm. The results of water extraction from airborne polarimetric SAR images are not ideal.

In order to eliminate the interference of low scattering intensity targets on the water extraction of airborne polarimetric SAR, this paper proposes a method of fine water extraction incorporating the relative difference of eigenvalues. Firstly, the weak scattering objects are extracted based on H-α Wishart [10] classification algorithm, and then, the weak scattering objects are segmented based on the pre-classification results. Then, we construct the single bounce eigenvalue relative difference [11, 12] (SERD) feature of the image and use the threshold method to screen out the water target from the weak scattering object unit. In order to verify the validity of the proposed algorithm, the full polarization SAR images of Nanchong City obtained from UAV SAR system were tested.

2 Construction of Weak Scattering Object Unit

In airborne SAR images, the weak scattering objects are seriously affected by speckle noise. If only processed at the pixel level, the results will be fragmented, and the image points will be isolated. Therefore, based on H-α Wishart pre-classification results, this paper constructs objects based on fractal network evolution algorithm.

The fractal network evolutionary segmentation algorithm is a bottom-up segmentation strategy. The basic idea is to merge pixels or objects in the direction of decreasing heterogeneity until the increment of heterogeneity after merging exceeds the threshold, and then, the merging terminates. The traditional fractal network evolutionary segmentation method uses spectral information and shape information to describe the heterogeneity of objects. Spectral information and shape information of various polarization features are integrated to describe the heterogeneity of objects and are used to segment polarization SAR buildings. The principle is as follows:

Suppose that before merging, object 1 contains n_1 pixels, heterogeneity is h_1, object 2 contains n_2 pixels, heterogeneity is h_2, and merged object heterogeneity is

h_m. The variation of heterogeneity before and after merger is as follows:

$$h_{\text{diff}} = (n_1 + n_2)h_m - (n_1 h_1 + n_2 h_2) = n_1(h_m - h_1) + n_2(h_m - h_2) \quad (1)$$

A K-dimension feature participates in the segmentation, assigns a weight w_k to each dimension feature and describes the heterogeneity with the standard deviation of the eigenvalue in the object, and then the variation of the heterogeneity of the object's feature becomes as follows:

$$h_{\text{pol}} = \sum_k w_k(n_1(\sigma_m - \sigma_1) + n_2(\sigma_m - \sigma_2)) \quad (2)$$

Shape heterogeneity is generally defined in terms of compactness and smoothness. If the compactness and smoothness of the segmented object are h_{cmpt} and h_{smooth}, respectively, the shape heterogeneity h_{shape} can be expressed as follows:

$$h_{\text{shape}} = w_{\text{cmpt}} h_{\text{cmpt}} + \big(1 - w_{\text{cmpt}}\big)h_{\text{smooth}} \quad (3)$$

Let the weight of feature heterogeneity be w_{pol}. Then, the similarity F of adjacent image objects can be expressed as:

$$f = w_{\text{pol}} h_{\text{pol}} + \big(1 - w_{\text{pol}}\big)h_{\text{shape}} \quad (4)$$

3 Fine Extraction of Water Body Integrating SERD

SERD is calculated from the average coherence matrix satisfying the assumption of reflection symmetry. In addition to reflection symmetry, it is stipulated that for natural media, the correlation between the same polarization channel and the cross polarization channel can be assumed to be zero. Based on the S matrix satisfying the reflection symmetry, the expression of the corresponding unsorted eigenvalues is derived as follows:

$$\begin{aligned}
\lambda_1 &= \frac{1}{2}\left\{ |S_{HH}|^2 + |S_{VV}|^2 + \sqrt{\left(|S_{HH}|^2 - |S_{VV}|^2 + 4\left|S_{HH}S_{VV}^*\right|^2\right)} \right\} \\
\lambda_2 &= \frac{1}{2}\left\{ |S_{HH}|^2 + |S_{VV}|^2 - \sqrt{\left(|S_{HH}|^2 - |S_{VV}|^2 + 4\left|S_{HH}S_{VV}^*\right|^2\right)} \right\} \\
\lambda_3 &= 2|S_{HV}|^2 \\
\text{SERD} &= \frac{\lambda_s - \lambda_3}{\lambda_s + \lambda_3}
\end{aligned} \quad (5)$$

In the formula, λ_s corresponds to the eigenvalue of single scattering, and α_i is the parameter α extracted from the eigenvector corresponding to λ_i. When $\alpha_1 \leq \frac{\pi}{4}$ or $\alpha_2 \geq \frac{\pi}{4}$, $\lambda_s = \lambda_1$; when $\alpha_1 \geq \frac{\pi}{4}$or $\alpha_2 \leq \frac{\pi}{4}$, $\lambda_s = \lambda_2$.

Influenced by surface roughness, the soil is characterized by low-entropy scattering in long-wavelength SAR images, while in Ku-band polarimetric SAR images, the soil is not dominated by Bragg scattering but by medium–low entropy. For water body, paddy field and road, because the scattering intensity of each channel is relatively low and close and affected by coherent speckle noise of the system, SAR images in Ku-band always show high entropy scattering characteristics, while SERD parameters are very useful for medium with high polarization entropy, which can determine the characteristics and magnitude of different scattering mechanisms.

4 Experimental Results and Analysis

4.1 Experimental Data

This paper makes use of the full polarization SAR data acquired by the unmanned aerial vehicle (UAV) airborne SAR system of Southwest China Research Institute of Electronic Equipment to carry out experiments on the fine extraction method of water body.

The UAV airborne SAR system operates in Ku-band with an incident angle ranging from 20 to 60 degrees. The working mode is strip imaging mode. The resolution of range and azimuth is 0.3 m. The maximum relative flight altitude is 3 km. The UAV-borne SAR system can support flight at altitude of 5 km. The maximum operating distance is 6 km, the maximum mapping bandwidth is 3 km, and it has *HH*. Full polarization measurement capability of *HV*, *VH* and *VV* is shown in Fig. 1a.

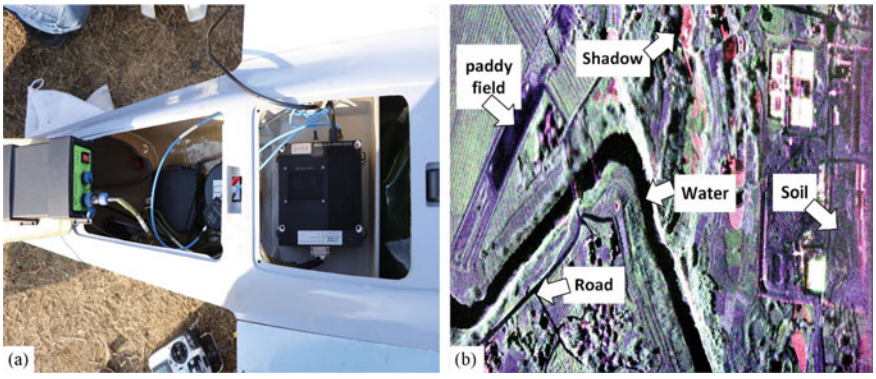

Fig. 1 Experimental data profiles. **a** UAV airborne SAR system. **b** Pauli RGB image

The full polarization SAR data obtained from the flight test of the UAV-borne SAR system in Nanchong in January 2018 were used to intercept a 6200 × 5400 pixel size area in the airstrip ID5, as shown in Fig. 1b Pauli RGB image. In Fig. 1b, in addition to water, weak scattering objects include shadows caused by houses and vegetation during crop growth, paddy fields, suburban roads and soil.

4.2 *Pre-classification and Construction of Weak Scattering Objects*

In order to satisfy the better interpretation effect, refined Lee filtering (filter window is 7*7) is applied to the image. Then, H-α Wishart classification is carried out in the experimental area, and the classification results are shown in Fig. 3. Even if the anisotropy parameter is added, it is still impossible to distinguish the weak scattering objects, and there are still a lot of weak scattering interference in the water extraction results. This is due to the following two reasons: (1) due to speckle noise interference, pixel-level results are difficult to distinguish weak scattering objects, but due to the impact of echo noise, the object based on the initial image is greatly disturbed. (2) In SAR images acquired under UAV SAR system, due to the large incidence angle of radar wave, the weak scattering objects show similar polarization scattering characteristics and are easy to be confused.

On the basis of the pre-classification results, this paper extracts the seventh kind of confused weak scattering objects from Fig. 2. Because of the large incidence angle, objects such as buildings, slopes and vegetation which are higher than the ground

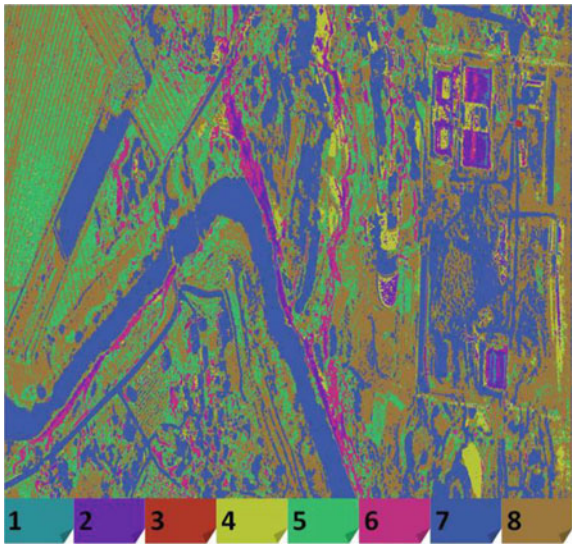

Fig. 2 H-α Wishart classification results in experimental areas

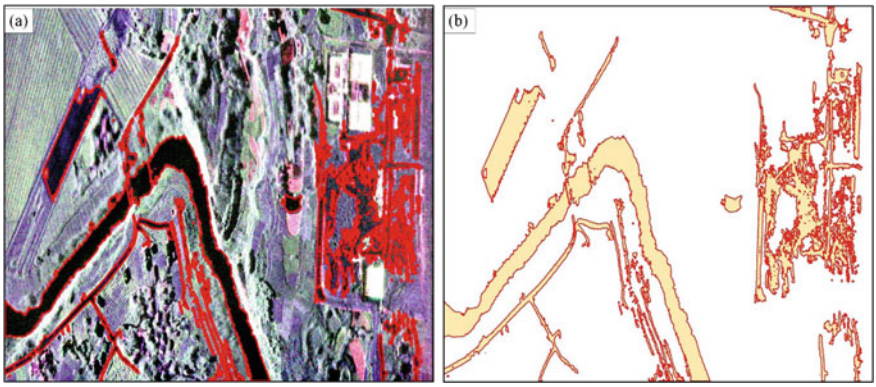

Fig. 3 Construction of weak scattering objects. **a** Overlapping Pauli RGB image of weak scattering objects. **b** Vector of weak scattering object

are easily affected by shadows. Because shadows do not contain or contain a small amount of information, shadows are often removed directly from the classification results without considering the impact of shadows. Airborne SAR images can get ground height by interferometry, so as to recognize and remove the shadow effects caused by buildings and other objects. This paper does not focus on this, so the shadow can be removed directly from seven categories. Using the extracted weak scattering objects to construct a mask, the polarization data are segmented by fractal network evolution under the restriction of the pre-segmentation class, and the object unit of weak scattering objects analysis is constructed, as shown in Fig. 3.

4.3 Fine Water Extraction by Introducing SERD

There are two steps in water body fine extraction: (1) initial determination of threshold based on histogram of SERD characteristics; (2) fine adjustment of threshold based on actual distinguishing results of objects to achieve fine extraction of water body.

The dynamic range of SERD is −1 to +1. It can be seen from Fig. 4a that the SERD value of water body is at a lower level than other low scattering objects. Using JET imaging, it can be seen that the color of water body region transits between yellow and red, while the color of other roads, paddy fields and bare soil is yellow–green to blue. There is a large SERD difference between water and non-water bodies during the transition. In order to distinguish water from non-water from weak scattering objects, SERD is masked by weak scattering classes, and the image shown in Fig. 4a is obtained. The distribution of SRED eigenvalues in Fig. 4a is counted, and the gray distribution in Fig. 4b is obtained. In Fig. 4b, there is an obvious double peak in the gray level distribution. The SERD value at the boundary between the two peaks is −0.3 as the initial threshold of judgment. In order to obtain a better separation effect,

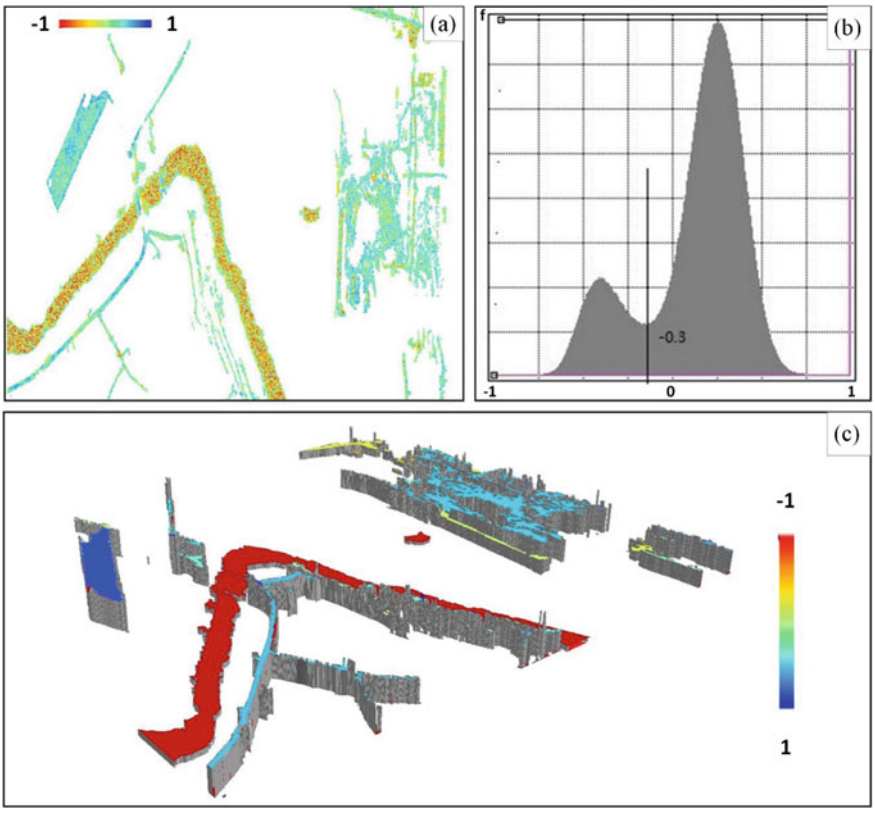

Fig. 4 SERD characteristic image. **a** SERD characteristics under pre-classification mask. **b** SERD histogram under pre-classification mask. **c** Object-level SERD height image

the SERD threshold was finally determined to be = 0.35 by fine-tuning the threshold according to the distinguishing effect between water and non-water. In Fig. 4c, the object is imaged to the JET color bar according to the object mean of SERD, and the object mean of SERD is also highly reflected.

On the premise of the same segmentation threshold, the precise extraction results of water body are obtained by using the pixel as the analysis unit and the object as the analysis unit, as shown in Fig. 5. As can be seen from the figure, the result of pixel level is not ideal because of speckle noise. There are not only isolated and misclassified pixel points, but also a considerable part of water body is not separated from non-water body, which makes the boundary of water body extraction result fragmented and confused. The results of the object as an analysis unit are not affected by speckle noise. The classification of water body and non-water body is realized. The boundary of the water body results is accurate and clear.

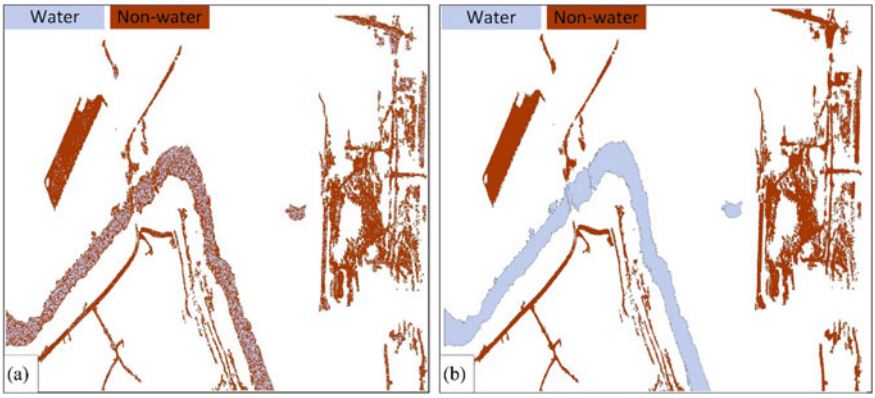

Fig. 5 Fine water extraction results. **a** Pixel-level water results. **b** Object-level water results

5 Conclusion

In this paper, the problem of object aliasing in high-resolution Ku-band airborne SAR system in water extraction is studied and discussed. In view of the fact that conventional spaceborne polarimetric SAR water extraction algorithm cannot distinguish water from weak scattering objects, this paper proposes a new method of fine water extraction incorporating SERD. Axis is pre-classified, fractal network evolution is used to segment weak scattering objects in pre-classification to obtain object-level analysis units; SERD eigenvalues of polarimetric SAR are calculated under pre-classification masks, and objects are taken as analysis units, and water body is fine extracted by threshold of SERD gray analysis, and other weak scattering objects are eliminated. In the future, we intend to do in-depth research and analysis on the adaptability of the algorithm with more data from different sources.

References

1. Fulong C, Hong Z, Chao W (2007) The Art in SAR Chang detection—a systematic review[J]. Remote Sens Technol Appl 22(1):109–115
2. Fan W, Chao W, Hang Z (2005) Residential area extraction from high resolution SAR images based on texture features[J]. Remote Sens Technol Appl 20(1):148–152
3. Changli Zheng, Guoman Huang, Zheng Zhao et al (2018) Water segmentation using multi-scale level set method based on joint distribution of G0 and Gamma [J]. Remote Sens Inf 33(1):13–20
4. Chuan Xu, Feng Hua, Haigang Sui et al (2014) Automatic segmentation of water from multi-scale level set SAR images [J]. J Wuhan Univ (Inf Sci Ed.) 39(1):27–31
5. Xiao C (2012) Research on extraction algorithms of flood and snow disaster area based on SAR image [D]. Univ Electron Sci Technol

6. Refice A, Capolongo D, Pasquariello G et al (2014) SAR and InSAR for flood monitoring: examples with COSMO-SkyMed data[J]. IEEE J Sel Top Appl Earth Obs Remote Sens 7(7):2711–2722
7. Lu J, Li J, Chen G et al (2017) Improving pixel-based change detection accuracy using an object-based approach in multitemporal SAR flood images[J]. IEEE J Sel Top Appl Earth Obs Remote Sens 8(7):3486–3496
8. Cossu R, Schoepfer E, Bally P et al (2009) Near real-time SAR-based processing to support flood monitoring[J]. J Real-Time Image Proc 4(3):205–218
9. Auynirundronkool K, Chen N, Peng C et al (2012) Flood detection and mapping of the Thailand central plain using RADARSAT and MODIS under a sensor web environment[J]. Int J Appl Earth Obs Geoinf 14(1):245–255
10. Ferro-Famil L, Pottier E, Lee J-S (2001) Unsupervised classification of multifrequency and fully polarimetric SAR images based on the H/A/A-wishart classifier[J]. IEEE Trans Geosci Remote Sens 39(11):2332–2342
11. Allain S, Ferrofamil L, Pottier E (2004) Two novel surface model based inversion algorithms using multi-frequency polSAR data[C]. IEEE Int Geosci Remote Sens Symp
12. Allain S, Lopez-Martinez C, Ferro-Famil L et al (2005) New eigenvalue-based parameter for natural media characterization[J]